Int. J. Heat Mass Transfer. Vol. 32, No. 2, pp. 321–334, 1989
Printed in Great Britain

0017–9310/89 $3.00 + 0.00

Viscous heating of a cylinder with finite length by a high viscosity fluid in steady longitudinal flow—1. Newtonian fluids

E. R. G. ECKERT and J. N. SHADID
Department of Mechanical Engineering, University of Minnesota, Minneapolis, MN 55455, U.S.A.

(*Received* 2 *February* 1988 *and in final form* 26 *May* 1988)

Abstract—The viscous dissipation heating of a finite length cylinder exposed to a steady uniform velocity Newtonian fluid is analyzed numerically. The solution determines the elliptic, velocity and temperature field, of a high viscosity fluid about an axisymmetric cylinder. Computations are performed for different values of the Reynolds number, Prandtl number, the probe radius to length ratio and the ratio of cylinder conductivity to fluid thermal conductivity. With polymer processing in mind the Reynolds number is varied between 10^{-4} and 2×10^{-1} and the Prandtl number between 10^5 and 10^9. The results also determine the increase in the cylinder wall and tip temperature due to viscous frictional heating. Strong elliptic effects on the velocity extend over 100 radius lengths upstream from the cylinder. The velocity field results indicate a nearly 'creeping flow' type velocity distribution about the cylinder body. In contrast, the temperature field is confined to a very narrow region of high deformation rates around the cylinder surface.

INTRODUCTION

THE EFFORT to measure local temperatures in a flowing polymer encounters the difficulty that any object exposed to a viscous flow is heated by internal friction in a process which converts mechanical energy in the fluid into internal energy and thus raises the probe temperature. This process is known as viscous heating. The resulting temperature increase has to be minimized or has to be determined by calibration if one wants to obtain from the recorded probe temperature the temperature which the fluid would have when the probe is absent.

This paper reports the results of an analysis of viscous heating of a cylinder with finite length oriented with its axis parallel to the velocity of the oncoming flow. It is thought that the cylinder approximates the shape of a temperature probe inserted into the fluid. The first part of the analysis presented in this paper considers a Newtonian fluid with constant properties as a limiting case of a non-Newtonian situation. The Reynolds number of the flow is postulated to be small and the Prandtl number of the fluid to be large to conform to the situation in polymer processing. The effects of the non-Newtonian nature of the fluid and of the temperature dependence of its properties will be investigated in a second paper.

The velocity and temperature fields are obtained by the analysis, in addition to the surface temperature of the cylinder. Knowledge of these fields is a prerequisite to an understanding of the relation between the temperature history of a polymer melt and its effect on the macroscopic physical properties of the polymer material. The present paper, therefore, also has interest in this context and it presents to our knowledge the first study of this kind in an external flow around an object, whereas internal flow situations for pipes, ducts, and extruders have been reported in the literature [1–7].

PROBLEM FORMULATION

The following equations describe the steady, laminar axisymmetric flow of a constant property Newtonian fluid past a cylinder arranged with its axis parallel to the main flow direction (Fig. 1). In the equations, the pressure work term in the energy equation and the gravity term in the momentum equation have been neglected. The equations have been made dimensionless by the following change of variables:

$$(x, r, u, v, P, \Theta) = \left(\frac{x^*}{R}, \frac{r^*}{R}, \frac{u^*}{U_0}, \frac{v^*}{U_0}, \frac{P^* R}{\eta U_0}, \frac{T^* - T_0}{\eta U_0 / \rho c_p R}\right). \tag{1}$$

The symbols are defined in the Nomenclature and are also indicated in Fig. 1. The resulting dimensionless equations are:

continuity equation

$$\frac{1}{r}\frac{\partial (rv)}{\partial r} + \frac{\partial u}{\partial x} = 0; \tag{2}$$

momentum equation

$$\frac{1}{2} Re \left(v\frac{\partial v}{\partial r} + u\frac{\partial v}{\partial x}\right) = -\frac{\partial P}{\partial r} + \frac{\partial}{\partial r}\left(\frac{1}{r}\frac{\partial (ru)}{\partial r}\right) + \frac{\partial^2 v}{\partial x^2} \tag{3}$$

$$\frac{1}{2} Re \left(v\frac{\partial u}{\partial r} + u\frac{\partial u}{\partial x}\right) = -\frac{\partial P}{\partial x} + \frac{1}{r}\frac{\partial}{\partial r}\left(r\frac{\partial u}{\partial r}\right) + \frac{\partial^2 u}{\partial x^2}; \tag{4}$$

NOMENCLATURE

c_p specific heat
$\mathbf{D}$ deformation rate tensor, $\frac{1}{2}(\nabla\mathbf{V}+\nabla\mathbf{V}^{\mathrm{T}})$
k thermal conductivity
L cylinder length
P^* pressure
P dimensionless pressure, $P^*R/\eta U_0$
Pr Prandtl number, $\eta c_p/k_f$
R cylinder radius
Re Reynolds number, $2\rho U_0 R/\eta$
r^* coordinate
r dimensionless coordinate, r^*/R
T^* temperature
T_0 upstream temperature
U_0 upstream velocity
u^* velocity component
u dimensionless velocity component, u^*/U_0
$\mathbf{V}$ velocity vector
v^* velocity component
v dimensionless velocity component, v^*/U_0
x^* coordinate measured from cylinder tip
x_c^* coordinate measured from cylinder midplane
x dimensionless coordinate, x^*/R.

Greek symbols
$\dot{\gamma}$ magnitude of deformation rate tensor $\mathbf{D}$
η viscosity
Θ temperature parameter, $(T^*-T_0)/(\eta U_0/\rho c_p R)$
θ angular coordinate
ρ density
Φ dissipation function
ψ stream function.

Subscripts
0 upstream
f fluid
p cylinder tip
s solid.

energy equation

$$\frac{1}{2}RePr\left(v\frac{\partial\Theta_f}{\partial r}+u\frac{\partial\Theta_f}{\partial x}\right)=\frac{1}{r}\frac{\partial}{\partial r}\left(r\frac{\partial\Theta_f}{\partial r}\right)+\frac{\partial^2\Theta_f}{\partial x^2}+\frac{1}{2}RePr\,\Phi \quad (5)$$

$$\Phi=2\left\{\left(\frac{\partial v}{\partial r}\right)^2+\left(\frac{v}{r}\right)^2+\left(\frac{\partial u}{\partial x}\right)^2\right\}+\left(\frac{\partial u}{\partial r}+\frac{\partial v}{\partial x}\right)^2. \quad (6)$$

With the boundary conditions for the computational domain ABCDEF:

on AB, CD

$$\frac{\partial u}{\partial r}=0,\quad v=0,\quad \frac{\partial\Theta_f}{\partial r}=0; \quad (7)$$

on AF, EF

$$u=1,\quad v=0,\quad \Theta_f=0; \quad (8)$$

on DE

$$\frac{\partial u}{\partial x}=\frac{\partial v}{\partial x}=\frac{\partial\Theta_f}{\partial x}=0; \quad (9)$$

on BG, HC

$$u=v=0,\quad \frac{\partial\Theta_f}{\partial x}=0; \quad (10)$$

on GH

$$u=v=0,\quad \frac{\partial\Theta_f}{\partial r}=0. \quad (11)$$

The boundary conditions on line segments AB and CD reflect the axisymmetric nature of the steady flow

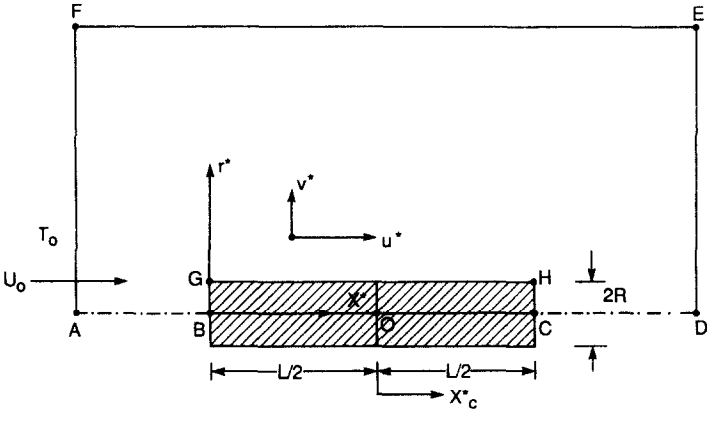

FIG. 1. Coordinate system and computational domain (not to scale).

past the cylinder. On segments AF and EF the flow conditions are taken to be free stream values since these boundaries are chosen to be far from the cylinder body. Outflow conditions are assumed to exist on segment DE which is located far downstream from the cylinder. At the solid–fluid interface made up of segments BG, GH and HC the no-slip condition holds along with the continuity of the interface temperature. It is also postulated that no temperature equalization occurs within the cylinder (the heat conductivity of the cylinder k_s is zero). The equation and boundary conditions show that the dimensionless velocity and pressure fields are functions of the Reynolds number, $Re = 2\rho RU_0/\eta$, and the geometric length parameter, R/L. The dimensionless temperature field depends in addition on the Prandtl number, $Pr = \eta c_p/k_f$. An average probe tip temperature, Θ_p, is defined as

$$\Theta_p = 2\int_0^1 \Theta|_{x=0}\, r\, dr. \tag{12}$$

In a later section the effect of internal equalization of the cylinder temperature is investigated. In this case equations (10) and (11) are changed to:

on BG, HC

$$u = v = 0, \quad \frac{k_s}{k_f}\frac{\partial \Theta_s}{\partial x} = \frac{\partial \Theta_f}{\partial x}; \tag{13}$$

on GH

$$u = v = 0, \quad \frac{k_s}{k_f}\frac{\partial \Theta_s}{\partial r} = \frac{\partial \Theta_f}{\partial r}; \tag{14}$$

and the Laplace equation for steady heat conduction in cylindrical coordinates is added to the system of equations (2)–(5) for the temperature field in the cylinder body.

COMPUTATIONAL DETAILS

The governing equations were discretized by using a control volume based finite difference scheme, the details of which can be found in ref. [8]. The SIMPLER procedure as given in ref. [8] was used for handling the flow field. The resulting system of non-linear algebraic equations was linearized by successive substitutions. At each iteration a direct inversion technique was used to solve for the flow variables (u, v, P), along with a line by line [8] technique for the temperature field Θ. A penalty method formulation is used to produce non-zero diagonal elements associated with the continuity equation in the coefficient matrix. This technique discussed in detail in ref. [9] allows efficient inversion of the coefficient matrix using sparse matrix routines.

The computational domain was discretized by a 150×50 non-uniform grid in the x, r-directions, respectively. The grid was finer in the x-direction at the probe tip, in the r-direction the grid was finest near the probe wall GH. In order to achieve grid and domain independent results a highly non-uniform grid was found to be necessary. There were essentially two reasons for this. First of all, the low Reynolds number effect of the diffusion terms dominating the inertia terms in the momentum equation caused a nearly 'creeping flow' type velocity distribution. Viscous effects were found to extend hundreds of radius lengths in all directions from the probe body. Therefore, in order to simulate a probe in an infinite fluid, it was necessary to increase the magnitudes of segments AB, AF, CD, DF, and EF until further movement of these boundaries produced negligible changes in the computed results. In practice this was carried out until further increases caused less than a $\frac{1}{2}$% change in the computed quantities. Domain independence test indicated non-dimensional lengths of 300 for $\overline{AB}$, $\overline{CD}$ and 200 for $\overline{AF}$, $\overline{DE}$.

In conflict with the need to discretize a large domain, the existence of large velocity gradients very close to the corner BGH necessitated the use of an extremely fine grid spacing at the corner to accurately resolve the production of thermal energy by viscous dissipation. In the grid independence studies it was determined that grid spacings of the order of 10^{-4}–10^{-5} were necessary to sufficiently resolve the high shear regions near the probe tip corner. This disparity of length scales was responsible for the large number of grid points used and the highly non-uniform spacing of the computational grid. The computations were performed on the Minnesota Supercomputer Institute's Cray-2 machines. Typical execution times for the numerical solutions were of the order of 500 s, the core memory required was about 5×10^6 Cray-2 words (64 bit words).

The influence of the non-dimensional parameters on the solution of the governing equations was determined as follows. For the case of an adiabatic probe ($k_s/k_f = 0$) the effect of Re on the velocity and temperature fields was studied by varying Re from 10^{-4} to 2×10^{-1}, while Pr and R/L were kept at 5×10^7 and 0.1, respectively. The value of Pr was varied from 10^5 to 10^9 for $Re = 10^{-2}$ and $R/L = 0.1$ to study its effect on the temperature field. With $Re = 10^{-2}$ and $Pr = 5 \times 10^7$ the geometric length ratio R/L was varied from 0.01 to 0.15. In order to analyze the influence of the thermal conductivity ratio on the fluid and solid temperature distribution, k_s/k_f was varied from 10^{-2} to 10^5 with Re, Pr, and R/L maintained at 10^{-2}, 5×10^7, and 0.1, respectively.

RESULTS AND DISCUSSION

Velocity field

A streamline plot of the flow field near the cylinder tip is presented in Fig. 2. The vertical and the horizontal scales are nonlinear and vary as $\sqrt{r}$ and $\sqrt{(|x - x_c|)}$, respectively. In this plot, as in others that follow, the axisymmetric nature of the flow has been used to present results for the entire plane $\theta =$

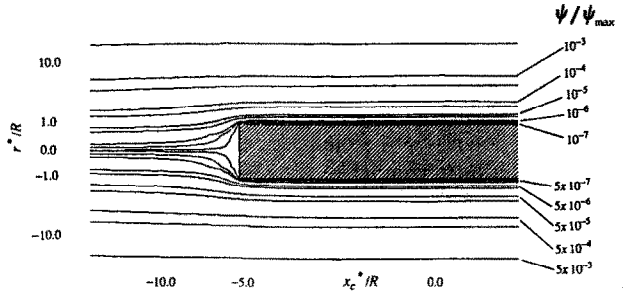

FIG. 2. Streamlines around the upstream half of a cylinder ($R/L = 10^{-1}$, $Re = 10^{-2}$, $Pr = 5 \times 10^7$).

constant. It is evident from the relative spacings of the streamlines, that as the fluid flows past the probe corner BGH it experiences a significant amount of acceleration. This strong acceleration, or equivalently in Eulerian terms, this large velocity gradient, is a major source of viscous dissipation heating near the probe tip. Along the body of the probe, the streamlines appear nearly parallel to the probe wall indicating a flow in which inertia effects are small in comparison with the viscous effects. This 'creeping flow' or 'Stokes flow' situation in which inertia forces are negligible relative to the viscous and pressure forces is characteristic of such low Reynolds number flows. The effect of Re on the symmetry of the flow about the midplane ($r\theta$-plane at O in Fig. 1) can be clearly observed in Fig. 3. In this figure, lines of constant

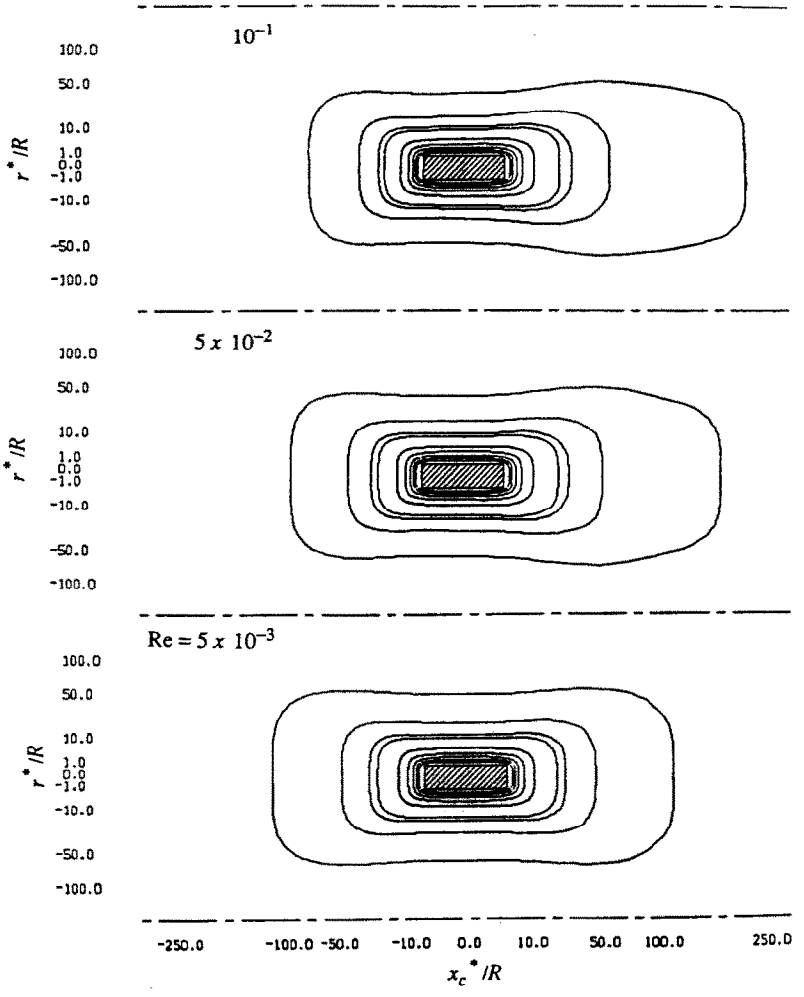

FIG. 3. Constant velocity contours for differing values of Reynolds number for $u^*/U_0 = 0.99, 0.95, 0.90, 0.875, 0.75, 0.625, 0.50, 0.375, 0.25$ ($R/L = 10^{-1}$, $Pr = 5 \times 10^7$).

velocity have been plotted about the probe body. The outermost contours have a value of $u^*/U_0 = 0.99$ and therefore represent the axisymmetric location of the 99% boundary layer. In the case $Re = 5 \times 10^{-3}$, the essentially symmetric distribution of velocity contours about the midplane is evident. As Re is increased, the location of the 99% boundary becomes convected or shifted downstream by the influence of the inertial forces. This effect however, decreases as the cylinder surface is approached indicating that in this region the viscous forces dominate the inertial forces even at $Re = 10^{-1}$. Postulating the flow as creeping should, therefore, be acceptable for the calculation of wall shear stress and heat transfer.

The upstream elliptic effects are clearly evident in the velocity profiles and the profiles of the deformation rate $\dot{\gamma}$ presented in Figs. 4 and 5. In Fig. 4, the profiles present the non-dimensional u component with respect to the non-dimensional radial distance from the cylinder axis. The viscous effects extend to a distance of about 70 in the r-direction and about 100 in the negative x-direction. A plot of the magnitude $\dot{\gamma}$ of the deformation rate tensor $\mathbf{D}$ is presented in Fig. 5. This parameter is also called the 'shear rate' for flows of generalized Newtonian fluids in which the viscosity η is allowed to vary with $\dot{\gamma}$. This will be the case for the fluids considered in the second paper. Equation (5) indicates that $\dot{\gamma}$ determines the amount of energy converted from mechanical to internal energy since $\Phi = 2\dot{\gamma}^2$, which is also true of all generalized Newtonian fluids. In Fig. 5, it is apparent that the location of the maximum deformation rate shifts from the stagnation point streamline ($r = 0$) upstream from the cylinder body to the corner BGH at the cylinder tip. The shift of the location of the maximum shear rate towards ($r = 1$) is accompanied by a corresponding decrease in the stagnation streamline shear rate magnitude. The region of high deformation rate becomes narrower as the corner of the cylinder is approached. Since the viscous dissipation source term is essentially given by the deformation rate magnitude $\dot{\gamma}$, it is expected that the deformation rate distribution will be of primary importance in development of the steady temperature field Θ_f.

Deformation rate profiles along the surface of the cylinder wall (for positive x^*/L values) are shown in Fig. 6. These profiles have been plotted for three locations symmetric with respect to the midplane O. The creeping flow type symmetry about the midplane is readily apparent. Velocity profiles along the cylinder surface show only a small change from the $x^*/R = 0$ profile in Fig. 4 and therefore they have not been presented.

Temperature field around the adiabatic cylinder

An isotherm plot of the temperature distribution around the upstream half of the cylinder is shown in Fig. 7. A comparison of the thickness of the velocity boundary layer (where $u^*/U_0 = 0.99$) to the distance of the isotherm in Fig. 7 for $\Theta_f = 10^{-2}$ indicates that the thermal boundary layer generated by viscous heating is much thinner than the velocity boundary layer.

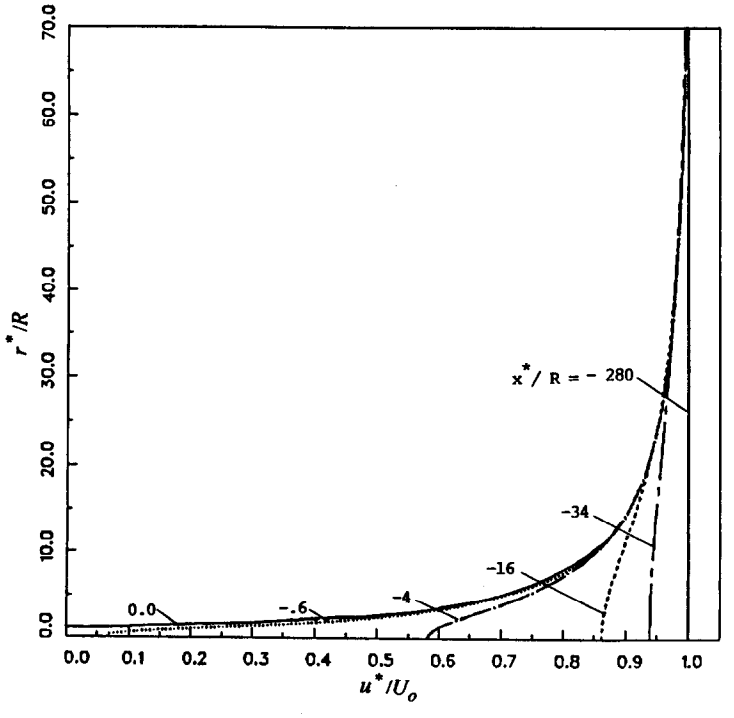

FIG. 4. Velocity field upstream of the cylinder tip ($R/L = 10^{-1}$, $Re = 10^{-2}$, $Pr = 5 \times 10^7$).

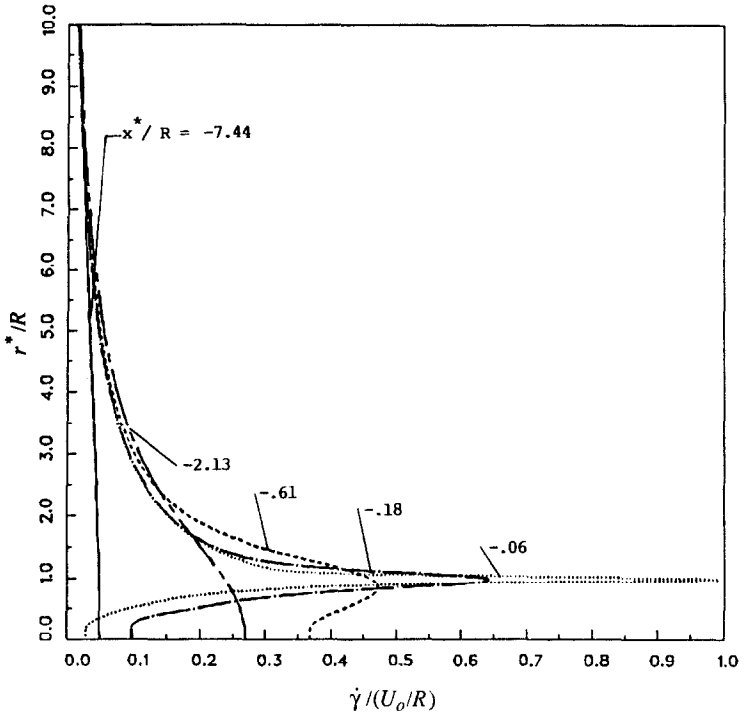

FIG. 5. Upstream profiles of the deformation rate $\dot{\gamma}$ ($R/L = 10^{-1}$, $Re = 10^{-2}$, $Pr = 5 \times 10^{7}$).

The reason for this appears to be the concentration of the deformation rate term $\dot{\gamma}$ near the surface and the large Prandtl number of the fluid. In Fig. 8, representative temperature profiles are presented at various x locations upstream of the adiabatic tip. The similarity to the deformation rate profiles in Fig. 5 is readily apparent. Similar to the thinning of the maximum shear layer, the temperature profile undergoes a noticeable increase in temperature at the corner ($r = 1$) of the cylinder tip. Corresponding

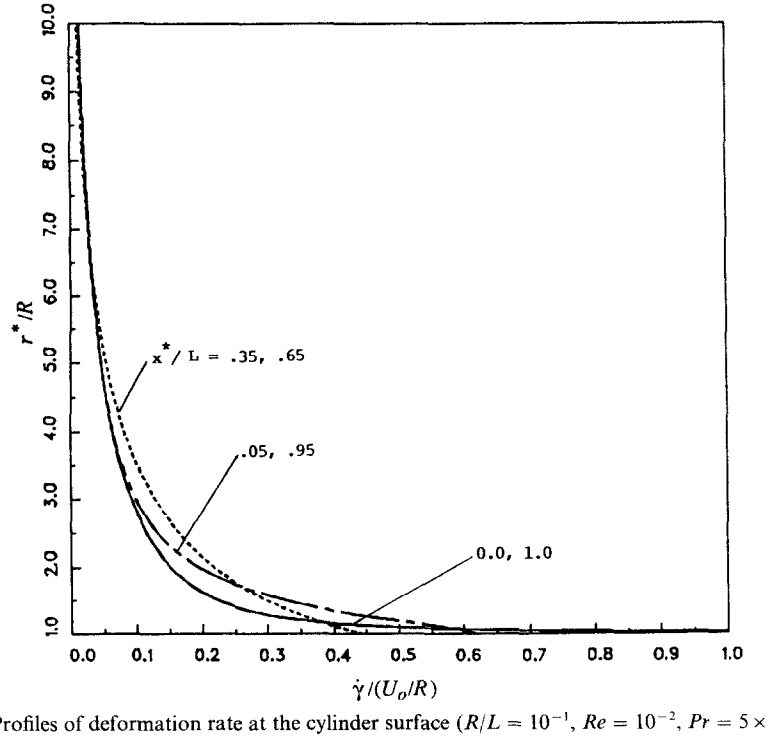

FIG. 6. Profiles of deformation rate at the cylinder surface ($R/L = 10^{-1}$, $Re = 10^{-2}$, $Pr = 5 \times 10^{7}$).

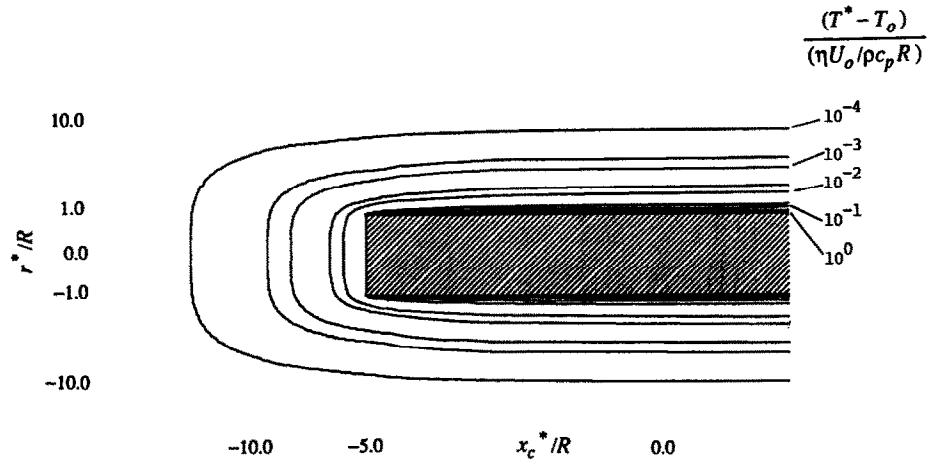

FIG. 7. Isotherms at the upstream half of the adiabatic cylinder ($R/L = 10^{-1}$, $Re = 10^{-2}$, $Pr = 5 \times 10^7$).

to the stagnation streamline deformation rate decrease, there is a significant decrease in production of thermal energy locally as the probe tip is approached. This decrease is associated with a limiting value $\Theta_f = 2.6$ of the temperature along the stagnation streamline.

Temperature profiles along the adiabatic probe surface are presented in Fig. 9. These results indicate an increase in local wall temperature on the adiabatic cylinder surface with increasing distance from the cylinder tip. The effect of the flow and geometrical parameters on this gradient are discussed in detail in the next section.

Cylinder wall and tip temperature

The effect of *Re*, *Pr* and *R/L* on wall temperature for an adiabatic cylinder are presented in Figs. 10–12. The effect of *Re* on the adiabatic wall temperature is shown in Fig. 10(a) for the case $R/L = 0.1$ and $Pr = 5 \times 10^7$. A significant increase in the dimensionless wall temperature gradient is evident as the *Re*

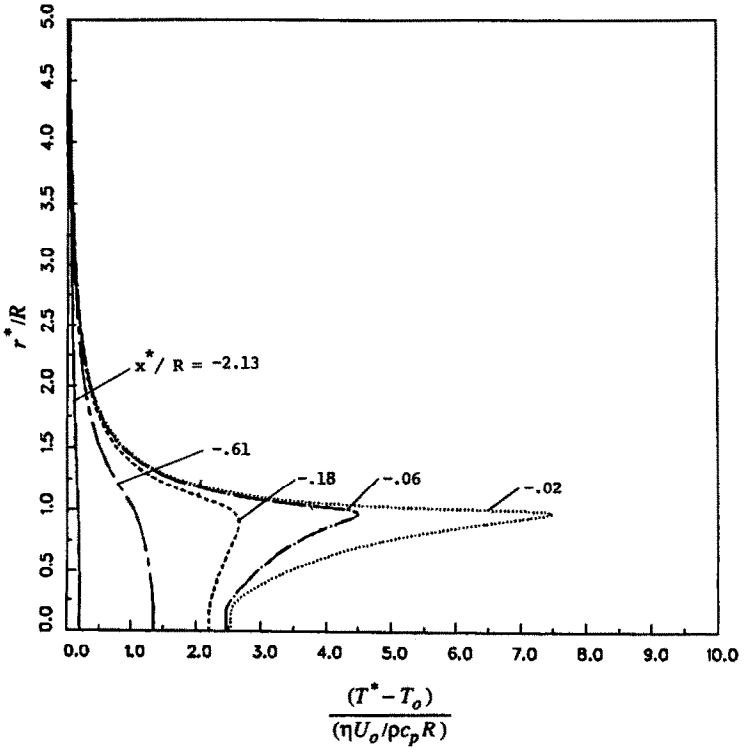

FIG. 8. Temperature profiles upstream of the adiabatic cylinder ($R/L = 10^{-1}$, $Re = 10^{-2}$, $Pr = 5 \times 10^7$).

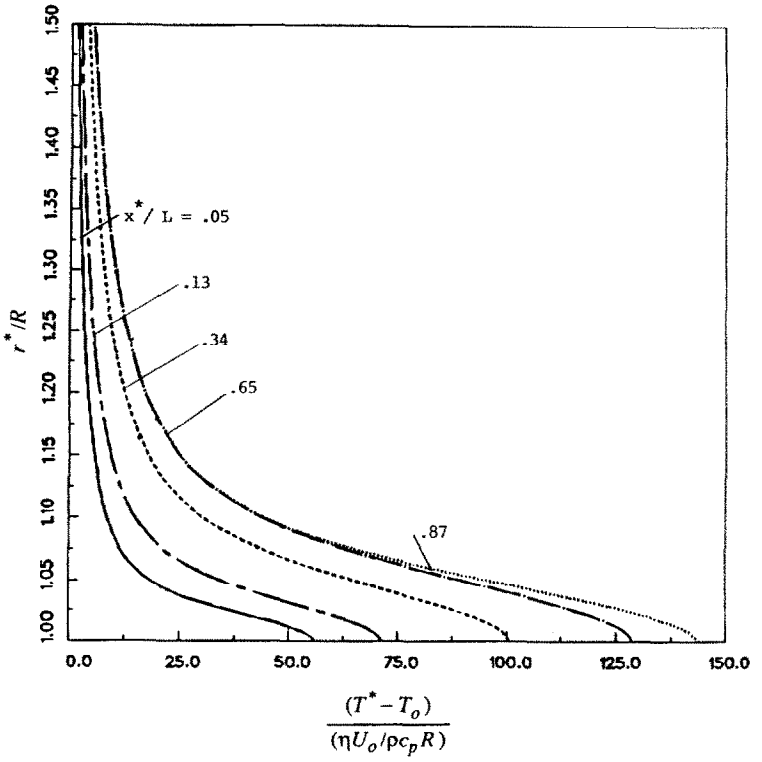

FIG. 9. Temperature profiles on the adiabatic cylinder surface ($R/L = 10^{-1}$, $Re = 10^{-2}$, $Pr = 5 \times 10^7$).

of the flow is increased. This is in contrast to a boundary layer situation (at large Re) on a plane surface where the adiabatic wall temperature is constant along the surface in the downstream direction. Figure 10(b) presents the influence of Re on the cylinder tip temperature Θ_p as defined by equation (12) for the same values of R/L and Pr. From this figure it is apparent that the influence of the inertial terms at low Reynolds numbers becomes small. Presumably for $Re < 10^{-4}$ there is a lower limit beyond which true creeping flow would exist and Re would cease to be an important parameter in the problem.

The effect of Pr on the cylinder wall and tip temperature is shown in Figs. 11(a) and (b) for $R/L = 0.1$ and $Re = 10^{-2}$. The functional form of this dependence and the magnitude of the influence is very similar to that of Re in Figs. 10(a) and (b).

The effect of the geometric length ratio R/L is presented in Figs. 12(a) and (b) for $Re = 10^{-2}$ and $Pr = 5 \times 10^7$. In the non-dimensional coordinates of Fig. 12(a) it is apparent that as R/L increases the wall temperature and wall temperature gradient decrease. This is essentially due to the fact that Re is based on the radius R and therefore a decreasing R/L (for a constant Re) implies a shorter probe, for which it is expected that a smaller temperature rise at a given x^*/L location would occur. The crossover point at small x^*/L is due to the fact that Θ_p is a weakly increasing function of R/L as shown in Fig. 12(b).

Effect of heat conduction in the cylinder

The results presented above have all been for the idealized case of an adiabatic cylinder. In reality the temperature distribution over the surface of the cylinder will be influenced by internal heat conduction in the cylinder. To exhibit the effect of the thermal conductivity of the cylinder material on the tip temperature and the temperature gradient, Figs. 13(a) and (b), have been included. Figure 13(a) shows the smoothing effects of an increase in the conductivity ratio k_s/k_f on the temperature gradient. As the cylinder becomes perfectly conducting, the probe temperature becomes uniform. This decrease in the temperature gradient is associated with a significant increase in the tip temperature Θ_p as shown in Fig. 13(b). The low k_s/k_f (insulated) and the high k_s/k_f (perfectly conducting cylinder) asymptotic limits are clearly evident.

Numerical example

The relations obtained in the preceding section will be used to calculate the error which a temperature probe, similar in shape to a cylinder, experiences in a steady, low Reynolds number and high Prandtl number fluid flow by viscous heating. The Newtonian constant properties used are chosen to reflect typical liquid polymer values. The kinematic viscosity of the fluid is postulated to have the value $v = 5\ \mathrm{m^2\,s^{-1}}$ (the

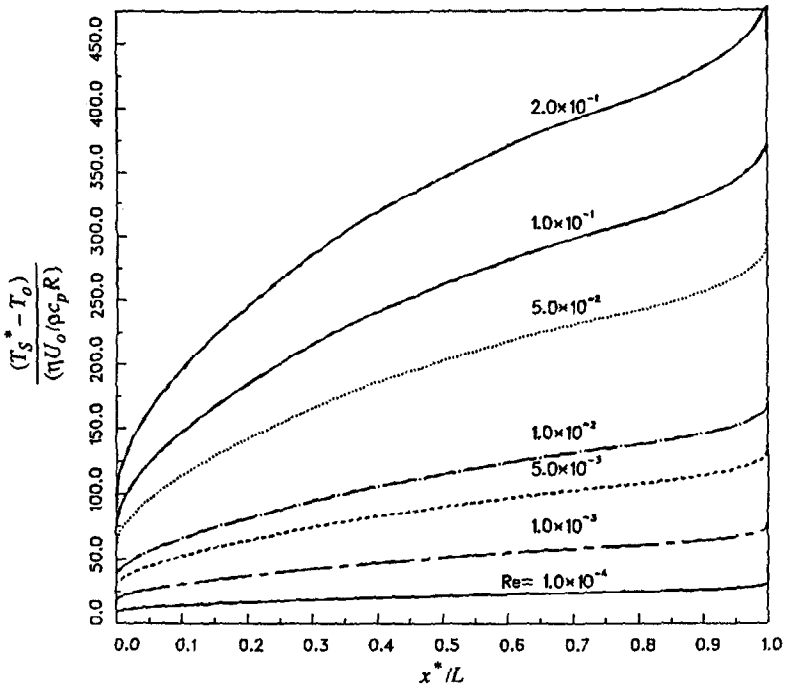

FIG. 10(a). Effect of Reynolds number on the local wall temperature of the adiabatic cylinder ($R/L = 10^{-1}$, $Pr = 5 \times 10^7$).

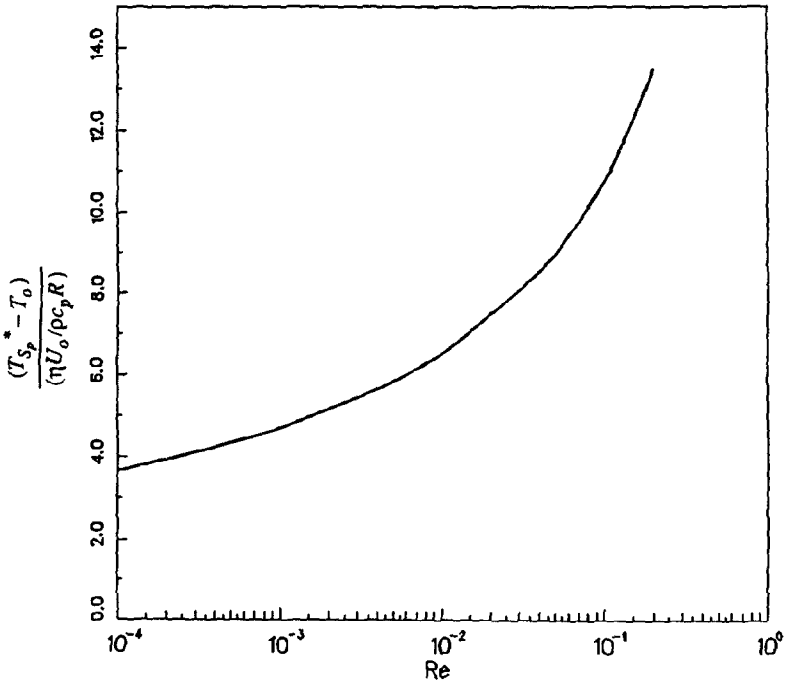

FIG. 10(b). Effect of Reynolds number on the tip temperature of the adiabatic cylinder ($R/L = 10^{-1}$, $Pr = 5 \times 10^7$).

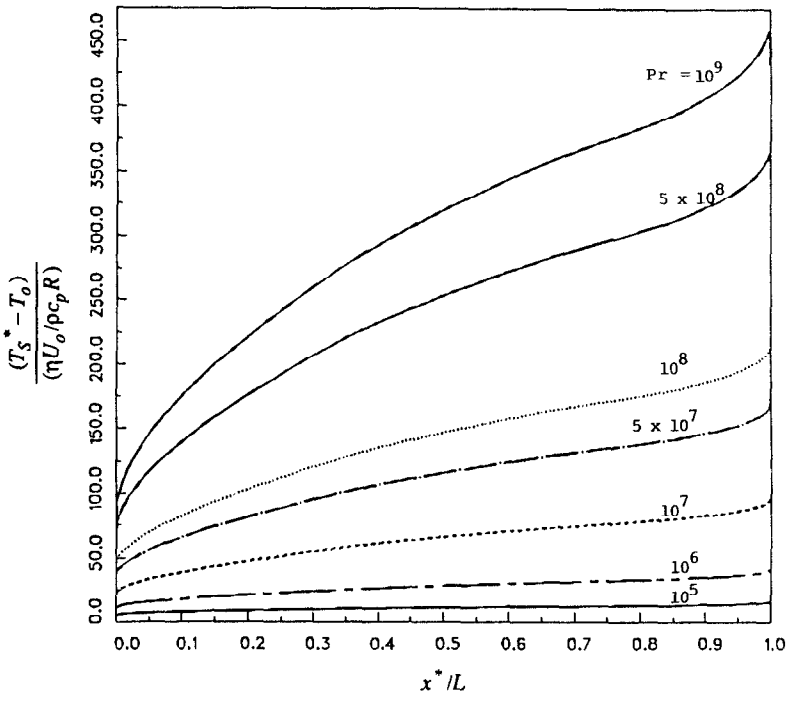

FIG. 11(a). Effect of Prandtl number on the local wall temperature of the adiabatic cylinder ($R/L = 10^{-1}$, $Re = 10^{-2}$).

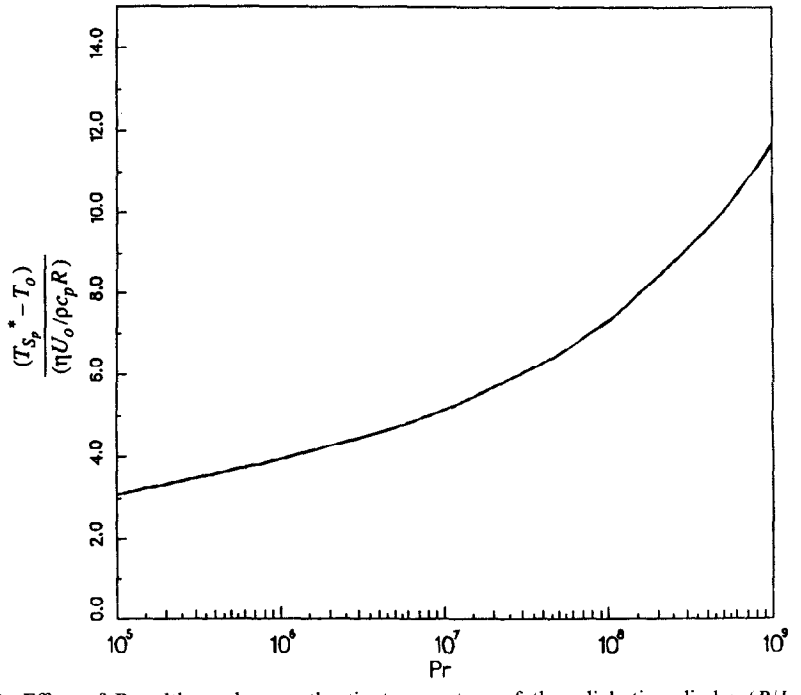

FIG. 11(b). Effect of Prandtl number on the tip temperature of the adiabatic cylinder ($R/L = 10^{-1}$, $Re = 10^{-2}$).

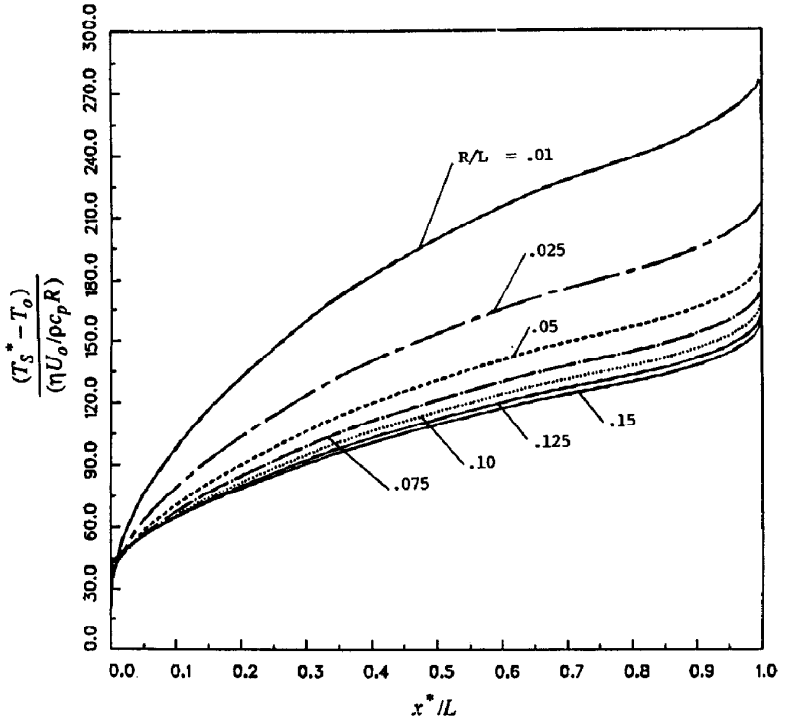

FIG. 12(a). Effect of R/L number on the local wall temperature of the adiabatic cylinder ($Re = 10^{-2}$, $Pr = 5 \times 10^7$).

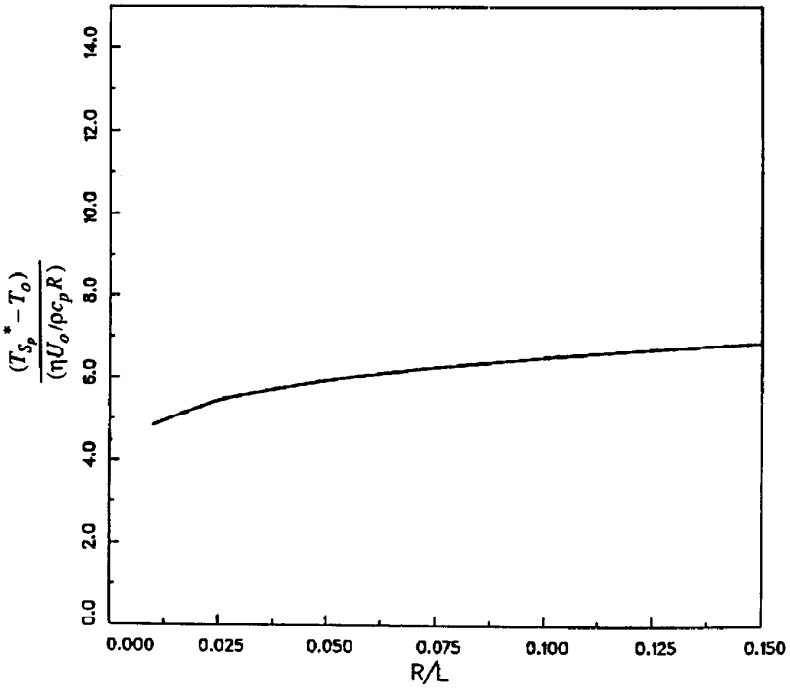

FIG. 12(b). Effect of R/L number on the tip temperature of the adiabatic cylinder ($Re = 10^{-2}$, $Pr = 5 \times 10^7$).

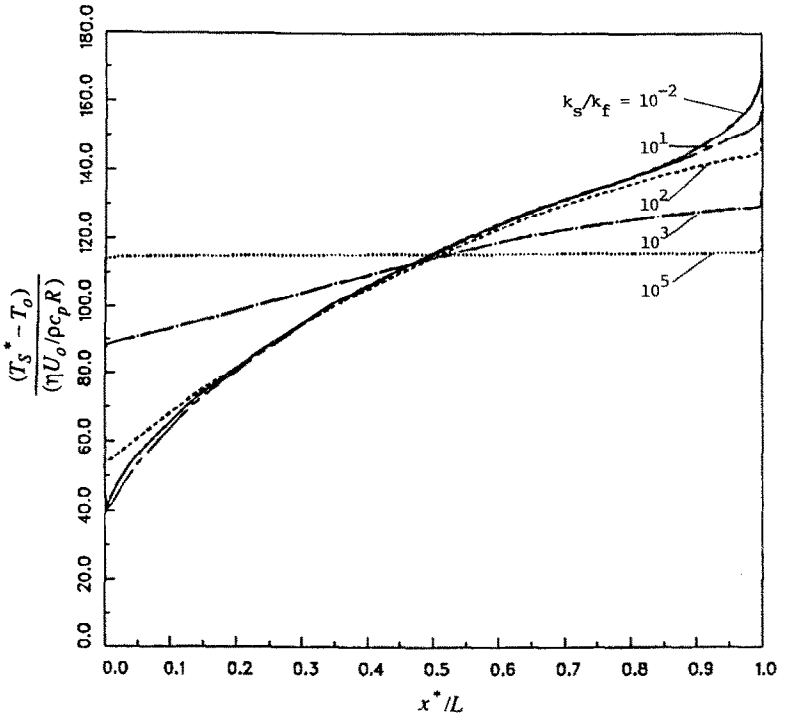

FIG. 13(a). Effect of conductivity ratio k_s/k_f on the local wall temperature of the cylinder ($R/L = 10^{-1}$, $Re = 10^{-2}$, $Pr = 5 \times 10^7$).

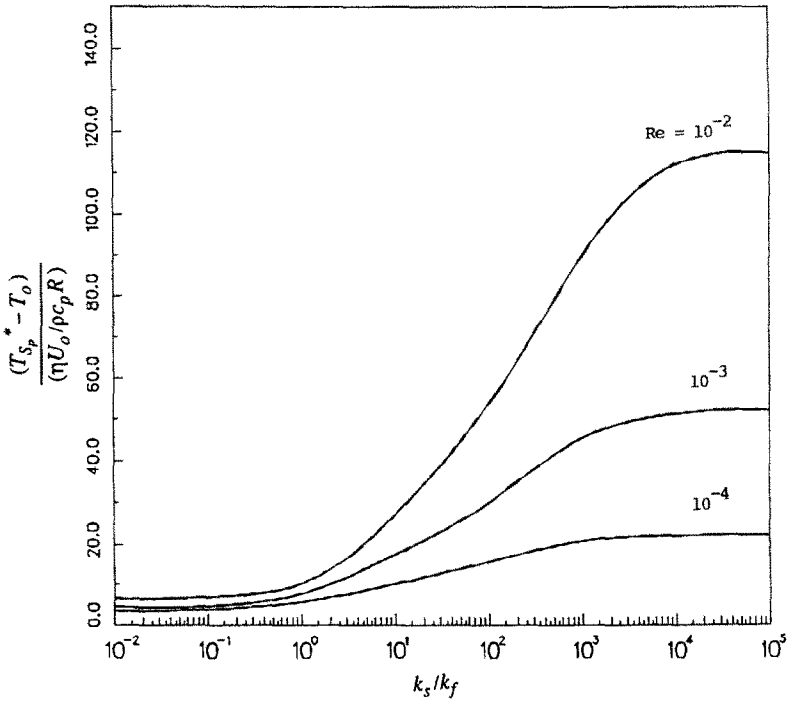

FIG. 13(b). Effect of k_s/k_f number on the tip temperature of the cylinder ($R/L = 10^{-1}$, $Pr = 5 \times 10^7$).

Table 1. Dependence of the temperature parameter Θ_p on the length ratio R/L ($Re = 10^{-3}$ and $Pr = 10^8$)

R/L	Adiabatic	Isothermal
0.050	4.72	74.34
0.025	4.37	85.50
0.010	4.01	106.60

range for polymers is of the order of 1–100 $m^2\ s^{-1}$) and its specific heat to be $c_p = 2 \times 10^3\ J\ kg^{-1}\ K^{-1}$.

The approach velocity of the fluid to the probe is assumed $U_0 = 1.0\ m\ s^{-1}$ and the diameter of the probe $2R = 5 \times 10^{-3}$ m. The Reynolds number of the flow is obtained with these values to be $Re = 10^{-3}$.

The error of the temperature probe, the difference between the dimensional tip temperature $T^*_{s_p}$ and the upstream fluid temperature T_0, is obtained from equation (12) to be

$$T^*_{s_p} - T_0 = \Theta_p \frac{2U_0^2/c_p}{Re}. \tag{15}$$

The temperature parameter Θ_p is obtained from Fig. 13(b). It has the value 4.75 for an adiabatic probe (without temperature equalization by internal heat conduction in the probe), and the value 52 for an isothermal probe (according to a probe heat conductivity of ∞). With the values listed above, the error of the temperature probe assumes the value 4.75°C for the adiabatic probe and 52.0°C for the isothermal probe. It is, therefore, important to reduce internal heat conduction by proper probe design. It should however be possible to approach the value for an adiabatic probe since the temperature parameter Θ_p increases only slightly for $k_s/k_f \leqslant 1$. A calibration of the temperature error or an estimate of its value using the preceding figures is probably required for the situation of this example to obtain sufficient accuracy of the temperature measurements. The temperature error is relatively insensitive to the ratio of probe radius R to probe length L as indicated in Table 1, in which the temperature parameter Θ_p of the probe tip is listed for an adiabatic and an isothermal probe. One will probably prefer to round off the tip of the temperature probe instead of the plane tip of the cylinder. This, however, should have a minor influence on the average temperature of the probe tip.

CONCLUDING REMARKS

A numerical analysis has been presented for steady, low Reynolds number flow of a high Prandtl number fluid for an adiabatic cylinder of finite length with its axis parallel to the main flow direction. The fluid is postulated to be Newtonian and to have properties which are independent of temperature. The effects of Reynolds number and Prandtl number as well as of the ratio of cylinder radius to its length on the velocity and temperature field, the probe wall and tip temperature are presented in a number of figures.

As expected, the viscosity dominated flow field extends hundreds of probe radii in all directions demonstrating the elliptic character of the equations describing the flow. Surprising, however, is the fact that the temperature field created by viscous dissipation is confined to a narrow region surrounding the cylinder. Both of these conditions cause the temperature along the probe surface to increase in the flow direction. In contrast, boundary layer solutions for plane flow over a flat surface at large Reynolds numbers result in a wall temperature which is constant in the flow direction [10].

The temperature gradients along the cylinder wall may generate heat conduction within the cylinder which tends to equalize its temperature. An additional calculation, therefore, considered the effect of internal heat conduction in the cylinder on the temperature variation along the cylinder wall and on the tip temperature.

A useful application of the analysis in this paper is the determination of the temperature error caused by viscous dissipation of the flow to which a temperature probe with a shape similar to the cylinder is exposed. Figures 13(a) and (b) and a calculated example indicate that it is important to minimize internal conduction in such a temperature probe when it is used to measure the temperature in a flowing polymer.

Acknowledgements—The computer time forming the basis of this research was supported by a grant from the University of Minnesota Supercomputer Institute.

REFERENCES

1. R. Nahme, Beitrage zur hydrodynamischen Theorie der Lagerreibung, *Ing.-Arch.* **11,** 191 (1940).
2. H. H. Winter, Viscous dissipation in shear flows of molten polymers. In *Advances in Heat Transfer*, pp. 205–267. Academic Press, New York (1977).
3. J. R. A. Pearson, Variable-viscosity flows in channels with high heat generation, *J. Fluid Mech.* **83,** 191–206 (1977).
4. J. R. A. Pearson, Polymer flows dominated by high heat generation and low heat transfer, *Polym. Engng Sci.* **18,** 222–229 (1978).
5. H. Ockendon, Channel flow with temperature dependent viscosity and internal viscous dissipation, *J. Fluid Mech.* **93,** 737–746 (1979).
6. S. A. Bostandzhiyan and A. M. Stolin, The critical conditions of the thermal regime of generalized Couette flow, *Inzh.-Fiz. Zh.* **17,** 86–94 (1969).
7. E. R. G. Eckert and M. Faghri, Viscous heating of high Prandtl number fluids with temperature-dependent viscosity, *Int. J. Heat Mass Transfer* **29,** 1177–1183 (1986).
8. S. V. Patankar, *Numerical Heat Transfer and Fluid Flow*. Hemisphere, New York (1980).
9. M. E. Braaten, Development and evaluation of iterative and direct methods for the solution of the equations governing recirculating flows, Ph.D. Thesis, University of Minnesota (1985).
10. E. R. G. Eckert and R. M. Drake, Jr., *Analysis of Heat and Mass Transfer*. McGraw-Hill, New York (1972).

CHAUFFAGE VISQUEUX D'UN CYLINDRE DE LONGUEUR FINIE, AVEC UN FLUIDE TRES VISQUEUX EN ECOULEMENT PERMANENT LONGITUDINAL—1. FLUIDES NEWTONIENS

Résumé—On étudie numériquement le chauffage par dissipation visqueuse d'un cylindre de longueur finie, exposé à un fluide newtonien ayant une vitesse uniforme et permanente. La solution détermine le champ elliptique de vitesse et de température pour un fluide très visqueux autour d'un cylindre axisymétrique. Des calculs sont effectués pour différentes valeurs du nombre de Reynolds, du nombre de Prandtl, du rapport rayon/longueur de la sonde et du rapport de la conductivité thermique du cylindre à celle du fluide. En pensant aux fluides polymères, le nombre de Reynolds est rendu variable entre 10^{-4} et 2×10^{-1}, et le nombre de Prandtl entre 10^5 et 10^9. Les résultats déterminent aussi l'accroissement de température de la paroi du cylindre et de l'extrémité, du fait du chauffage visqueux. Des effets elliptiques intenses sur la vitesse s'étendent jusqu'à des distances de 100 fois le rayon, en amont du cylindre. Les résultats sur le champ de vitesse montrent une distribution de vitesse proche du type "écoulement rampant" autour du cylindre. En contraste, le champ de température est confiné à la région très étroite des fortes vitesses de déformation autour du cylindre.

ERWÄRMUNG EINES ZYLINDERS MIT ENDLICHER LÄNGE DURCH DIE REIBUNGSHITZE IN EINEM FLUID HOHER VISKOSITÄT BEI STATIONÄRER AXIALER UMSTRÖMUNG—1. NEWTON'SCHE FLUIDE

Zusammenfassung—Die Erwärmung eines Zylinders endlicher Länge, der einer gleichmäßigen Strömungsgeschwindigkeit in einem Newton'schen Fluid ausgesetzt ist, wird numerisch untersucht. An einem achsensymmetrischen Zylinder in einem hochviskosen Fluid ergibt sich ein elliptisches Geschwindigkeits- und Temperaturfeld. Die Berechnungen wurden für verschiedene Reynolds- und Prandtl-Zahlen, Radius/Längen-Verhältnisse des Zylinders und verschiedene Verhältnisse der Wärmeleitfähigkeiten von Zylinder und Fluid durchgeführt. Im Hinblick auf die Polymer-Herstellung wurde die Reynolds-Zahl zwischen 10^{-4} und 2×10^{-1} und die Prandtl-Zahl zwischen 10^5 und 10^9 variiert. Zusätzlich ergibt die Berechnung auch eine Temperaturerhöhung an der Zylinderwand und -stirnseite durch die Reibungshitze. Die starke elliptische Verformung des Geschwindigkeitsprofils dehnt sich bis zum Hundertfachen der Zylinderlänge in das Zuströmgebiet aus. Die Ergebnisse des Geschwindigkeitsfeldes deuten auf eine Art schleichende Strömung an der Oberfläche des Zylinderkörpers hin. Im Gegensatz dazu bleiben die Veränderungen des Temperaturfeldes auf einen sehr schmalen Bereich an der Zylinderoberfläche beschränkt.

ВЯЗКОСТНЫЙ НАГРЕВ ЦИЛИНДРА КОНЕЧНОЙ ДЛИНЫ, ПРОДОЛЬНО ОБТЕКАЕМОГО СТАЦИОНАРНЫМ ПОТОКОМ ВЫСОКОВЯЗКОЙ ЖИДКОСТИ—1. НЬЮТОНОВСКИЕ ЖИДКОСТИ

Аннотация—Численно анализируется нагрев цилиндра конечной длины за счет вязкой диссипации при обтекании стационарным однородным потоком ньютоновской жидкости. Опредьлены эллиптические поля скорости и температуры высоковязкой жидкости вокруг осесимметрчного цилиндра. Расчеты выполнены при различных значениях чисел Рейнольдса и Прандтля, отношений радиуса зонда к его длине и отношений теплопроводностей цилиндра и жидкости. Число Рейнольдса изменялось в диапазоне от 10^{-4} до 2×10^{-1}, а число Прандтля—от 10^5 до 10^9, что характерно для технологии полимеров. Установлено увеличеие емпературы стенок и торцов цилидра, вызванное нагревом за счет вязкого трения. Сильное влияние эллиптичности поля на скорость распространяется вверх по течению от цилиндра на расстояние, равное более чем 100 радиусам цилиндра. Анализ поля скорости показал, что скорость вокруг цилиндрического тела распространяется по типу "ползучего течения". Температурное же поле ограничено очень узкой областью, где имеют место высокие скорости деформации вокруг поверхности цилиндра.